

WIMP Dark Matter Direct-Detection Searches in Noble Gases

Laura Baudis

Physik Institut, University of Zurich, Winterthurerstrasse 190, 8057 Zurich

Abstract

Cosmological observations and the dynamics of the Milky Way provide ample evidence for an invisible and dominant mass component. This so-called dark matter could be made of new, colour and charge neutral particles, which were non-relativistic when they decoupled from ordinary matter in the early universe. Such weakly interacting massive particles (WIMPs) are predicted to have a non-zero coupling to baryons and could be detected via their collisions with atomic nuclei in ultra-low background, deep underground detectors. Among these, detectors based on liquefied noble gases have demonstrated tremendous discovery potential over the last decade. After briefly introducing the phenomenology of direct dark matter detection, I will review the main properties of liquefied argon and xenon as WIMP targets and discuss sources of background. I will then describe existing and planned argon and xenon detectors that employ the so-called single- and dual-phase detection techniques, addressing their complementarity and science reach.

Keywords: dark matter, direct detection, noble gases, argon, xenon

1. Introduction

The motivation to build detectors that can directly detect particle dark matter in the laboratory comes from our current understanding of the observable universe. Cosmological observations ranging from the measured abundance of primordial elements to the precise mapping of anisotropies in the cosmic microwave background, to the study of the distribution of matter on galactic, extragalactic and the largest observed scales, to observations of high-redshift supernovae, have led to a so-called standard model of cosmology. In this model, our universe is spatially flat and composed of $\sim 5\%$ atoms, $\sim 27\%$ dark matter and $\sim 68\%$ dark energy [1]. Understanding the nature of dark matter poses a significant challenge to astroparticle and particle physics, for its solution may involve new particles with masses and cross sections characteristic of the electroweak scale. Such weakly interactive massive particles (WIMPs), which would have been in thermal equilibrium with quarks and leptons in the hot early universe, and decoupled when they were non-relativistic, represent a generic class of dark matter candidates [2]. Concrete examples are the lightest superpartner in supersymmetry with R-parity conservation [3], and the lightest Kaluza-Klein particle, for instance the first excitation of the hypercharge gauge boson, in theories with universal extra dimensions [4]. Perhaps the most intriguing aspect of the WIMP hypothesis is the fact that it is testable by experiment. WIMPs with masses around the TeV scale are within reach of high-energy colliders and of direct and indirect dark matter searches [5]. Axions and axion-like particles (ALPs), produced non-thermally in the early universe, represent another class of well-motivated dark matter candidates [6]. They can be searched for by exploiting their predicted couplings to photons and electrons, where the most successful technique to search for dark matter axions is the so-called axion haloscope, that relies on the axion to two-photon coupling [7, 8]. In this review I will focus on the search for WIMPs with low-background detectors operated underground.

2. Direct detection of WIMPs

Dark matter particles might be detected via their elastic collisions with atomic nuclei in earthbound, low-background detectors [9]. The differential rate for elastic scattering can be expressed as [10]:

$$\frac{dR}{dE_R} = N_T \frac{\rho_{dm}}{m_W} \int_{v_{\min}}^{v_{\max}} d\vec{v} f(\vec{v}) v \frac{d\sigma}{dE_R} \quad (1)$$

where N_T is the number of target nuclei, ρ_{dm} is the local dark matter density in the galactic halo, m_W is the WIMP mass, \vec{v} and $f(\vec{v})$ are the WIMP velocity and velocity distribution function in the Earth frame and $d\sigma/dE_R$ is the WIMP-nucleus differential cross section. The nuclear recoil energy is $E_R = m_r^2 v^2 (1 - \cos \theta) / m_N$, where θ is the scattering angle in the center-of-mass frame, m_N is the nuclear mass and m_r is the reduced mass. The minimum velocity is defined as $v_{\min} = (m_N E_{th} / 2m_r^2)^{\frac{1}{2}}$, where E_{th} is the energy threshold of the detector, and v_{\max} is the escape velocity in the Earth frame. The simplest galactic model assumes a Maxwell-Boltzmann distribution for the WIMP velocity in the galactic rest frame, with a velocity dispersion of $\sigma \approx 270 \text{ km s}^{-1}$ and an escape velocity of $v_{esc} \approx 544 \text{ km s}^{-1}$ [11, 12]. For direct detection experiments, the mass density and velocity distribution at a radius around 8 kpc are most relevant. State of the art, dark-matter-only cosmological simulations of Milky Way-like halos find that the dark matter mass distribution at the solar position is smooth, with substructures being far away from the Sun. The local velocity distribution of dark matter particles is likewise found to be smooth, and close to Maxwellian [13]. The efforts to measure the mean density of dark matter near our Sun are extensively reviewed in [14]: the Milky Way seems to be consistent with featuring a spherical dark matter halo with little flattening in the disc plane, and $\rho_{dm} = 0.2 - 0.56 \text{ GeV cm}^{-3}$ [14]. The largest source of uncertainty in ρ_{dm} comes from the baryonic contribution to the local dynamical mass.

The differential cross section for elastic scattering is traditionally split in two leading components: an effective scalar coupling between the WIMP and the mass of the nucleus and an effective coupling between the spin of the WIMP and the total angular momentum of the nucleus. In general, the coherent part dominates the interaction (depending however on the characteristics and composition of the dark matter particle) for target masses with $A \geq 30$ [3]. The total cross section is the sum of both contributions $\frac{d\sigma}{dE_R} \propto \sigma_{SI}^0 F_{SI}^2(E_R) + \sigma_{SD}^0 F_{SD}^2(E_R)$, where $\sigma_{SI,SD}^0$ are the spin-independent (SI) and spin-dependent (SD) cross sections in the limit of zero momentum transfer and $F_{SI,SD}^2(E_R)$ denote the nuclear form factors, expressed as a function of the recoil energy. These become significant at large WIMP and nucleus masses, leading to a suppression of the differential scattering rate at higher recoil energies. State-of-the art shell-model calculations for spin-dependent scattering were recently performed for most non-zero spin nuclei of interest in direct searches [15, 16]. In addition, in these new calculations the WIMP-nucleus currents are based on chiral effective field theory at the one-body level, and also include the leading long-range two-body currents.

Recent, more general treatments of the WIMP-nucleon cross section in non-relativistic, effective field theory approaches [17, 18, 19, 20], identify a full set of operators that describe the potential interactions of dark matter particles, and relate these to nuclear response functions. These are of great interest because, in principle, more information can be extracted from direct detection experiments in case of a signal detection, assuming a certain variety of targets is employed in the search.

Spin-dependent inelastic scattering offers an additional and complementary detection channel, in particular in nuclei with low-lying excited states in the energy range 10 – 100 keV. The experimental signature is a nuclear recoil together with the prompt de-excitation photon, boosting the region of interest to higher energies. Structure functions for inelastic WIMP-nucleus scattering are calculated in [21], showing that for momentum transfers around 150 MeV, the inelastic channel is comparable to, or can even dominate the elastic one. As an example, Figure 1 shows the differential recoil spectra for inelastic and elastic scattering off ^{129}Xe and ^{131}Xe (left), as well as the integrated inelastic and elastic rates (right), for 100 GeV WIMP with a WIMP-nucleon cross section of 10^{-40} cm^2 [21].

3. Backgrounds

A continuous challenge for direct dark matter search experiments is to minimize and accurately characterize the background noise. Some of the main background sources are the environmental radioactivity including airborne radon and its daughters, radio-impurities in the detector construction and shield material, neutrons from (α, n) and fission reactions, cosmic rays and their secondaries, and activation of detector

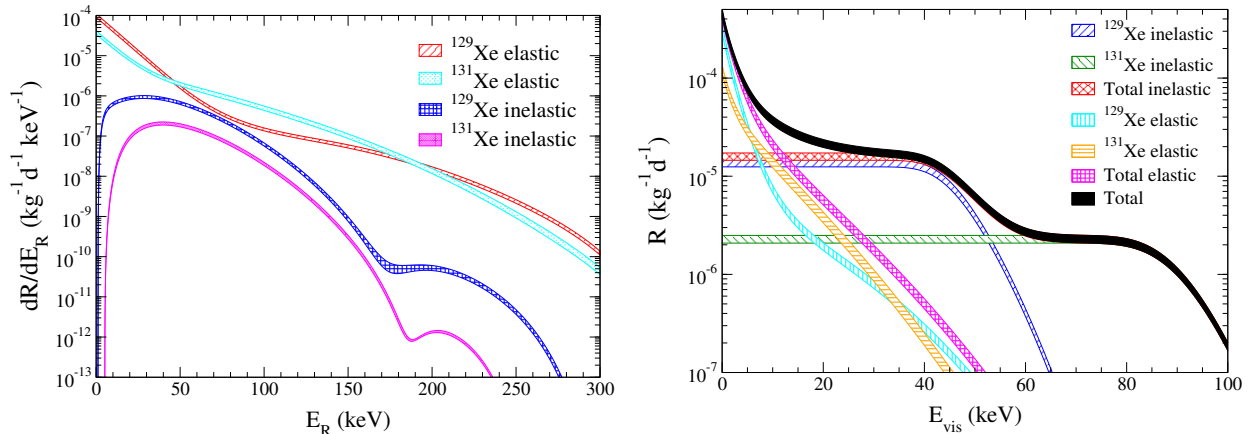


Figure 1: (Left) Differential nuclear recoil spectra as a function of recoil energy for scattering off ^{129}Xe and ^{131}Xe . Both elastic and inelastic recoil spectra are shown for comparison, the bands include the uncertainties due to WIMP-nucleon currents. (Right) Integrated energy spectra of xenon for elastic and inelastic, spin-dependent scattering. The inelastic contributions dominate over the elastic ones for moderate energy thresholds. A WIMP mass of 100 GeV, and a WIMP-nucleon cross section 10^{-40} cm^2 are assumed. Figure from [21].

materials during exposure at the Earth’s surface [22]. Background sources intrinsic to the detector materials, muon-induced high-energy neutrons and ultimately neutrinos start to play an increasingly important role already for the current generation of detectors.

In the past, a combination of low-Z and high-Z materials were employed to diminish the neutron and gamma fluxes coming from the laboratory walls and outer shield layers, and shield structures were kept under a N_2 -atmosphere at slight overpressure to suppress the background from airborne radon decays and subsequent ^{210}Pb plate-out. Detectors recently constructed or planned for the future increasingly use large water shields, which passively reduce the environmental radioactivity and muon-induced neutrons, and act as an active muon veto. Typical underground gamma- and radiogenic neutron fluxes of $0.3 \text{ cm}^{-2}\text{s}^{-1}$ and $9 \times 10^{-7} \text{ cm}^{-2}\text{s}^{-1}$, respectively [23] are reduced by a factor of 10^6 after 3 m and 1 m of water shield [24].

Critical are interaction from (α, n) - and fission neutrons from ^{238}U and ^{232}Th decays in detector components close to the dark matter target materials. The neutron energy spectra and yields are calculated using the exact composition of these materials and the measured amount of ^{238}U and ^{232}Th in each component. Because often secular equilibrium in the primordial decay chains is lost in processed materials, the ^{238}U and ^{232}Th activities are typically determined via mass spectrometry or neutron activation analysis, while the activities of the late part of these chains, ^{226}Ra , ^{228}Ac , ^{228}Th , are determined via gamma spectrometry using ultra-low background HPGe detectors [25]. The neutrons are then transported using Monte Carlo simulations to evaluate the expected number of single-scatter nuclear recoils, which might be difficult to distinguish from a potential WIMP signal [26].

In liquified noble gas detectors, sources of radioactivity intrinsic to the WIMP target materials such as ^{39}Ar , ^{85}Kr and radon diffusion provide challenging backgrounds for current and possibly future detectors. For instance, impurity levels of ~ 1 ppt in natural krypton and $\sim 1 \mu\text{Bq/kg}$ radon must be achieved by ton-scale experiments aiming to probe WIMP-nucleon cross sections down to 10^{-47} cm^2 , with typical expected background rates from external sources below 1 event per ton of target material and year.

The ultimate background source might be provided by the irreducible neutrino flux. Solar pp-neutrinos will contribute to the electronic recoil background via neutrino-electron scattering at the level of ~ 10 -25 events/(ton \times year) in the low-energy, dark matter signal region of a typical detector. Depending on the detector’s discrimination capabilities between electronic and nuclear recoils, solar pp-neutrinos may thus become a relevant background at cross sections $< 10^{-48} \text{ cm}^2$. Neutrino-induced nuclear recoils from coherent neutrino-nucleus scatters can not be distinguished from a WIMP-induced signal. The ^8B solar neutrinos yield up to 10^3 events/(ton \times year) for heavy targets such as xenon [28], however most of these events are

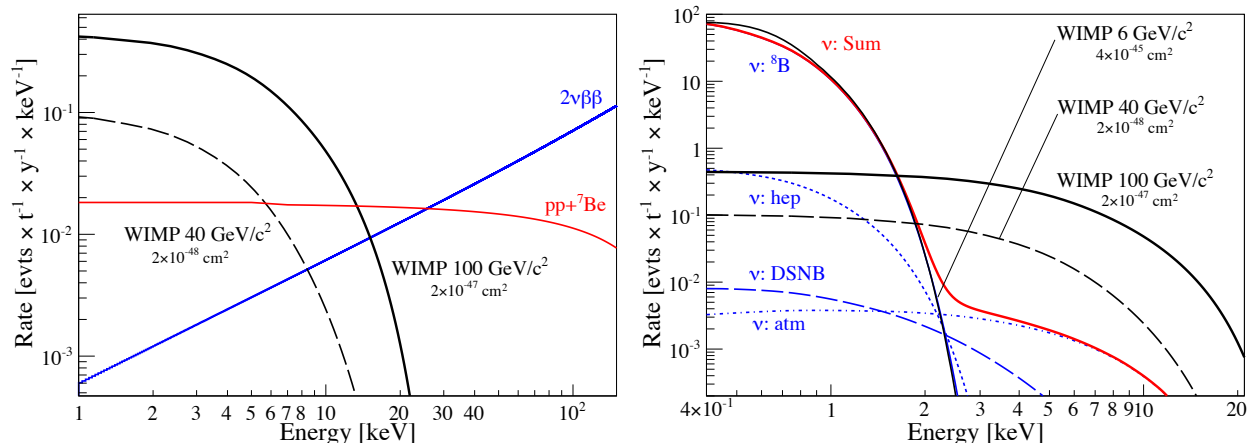


Figure 2: (Left) Summed differential energy spectrum for pp and ${}^7\text{Be}$ neutrinos (red) in a LXe detector. The electron recoil spectrum from the double beta decay of ${}^{136}\text{Xe}$ (blue), as well as the expected nuclear recoil spectrum from WIMP scatters for a spin-independent WIMP-nucleon cross section of $2 \times 10^{-47} \text{ cm}^2$ (solid black) and $2 \times 10^{-48} \text{ cm}^2$ (dashed black) and WIMP masses of $100 \text{ GeV}/c^2$ and $40 \text{ GeV}/c^2$ is also shown. A 99.5% discrimination of electronic recoils is assumed. (Right): The differential nuclear recoil spectrum from coherent scattering of neutrinos (red) from the Sun, the diffuse supernova background (DSNB), and the atmosphere (atm), compared to the one from WIMPs for various masses and cross sections (black). The coherent scattering rate will provide an irreducible background for low-mass WIMPs, limiting the cross section sensitivity to $\sim 4 \times 10^{-45} \text{ cm}^2$ for WIMPs of $6 \text{ GeV}/c^2$ mass, while WIMP masses above $\sim 10 \text{ GeV}/c^2$ will be significantly less affected. For both plots, the nuclear recoil signals are converted to an electronic recoil scale (see [27]) and a nuclear recoil acceptance of 50% is assumed. Figure from [27].

below the energy thresholds of current and likely also future noble liquid detectors. Nuclear recoils from atmospheric neutrinos and the diffuse supernovae neutrino background will yield event rates in the range 1-5 events/(100 ton \times year), depending on the target material, and hence will dominate measured spectra at a WIMP-nucleon cross section below 10^{-49} cm^2 [28, 29, 30, 31, 27]. Figure 2 shows the expected background spectrum from pp and ${}^7\text{Be}$ solar neutrinos (left), as well as from coherent scattering of solar, atmospheric and diffuse supernova background neutrinos (right) in a detector using xenon as target material. Also shown are predicted WIMP-induced differential nuclear recoil spectra for various WIMP masses and cross sections. The underlying assumptions are detailed in the figure caption, and in [27].

4. Liquefied noble gases as WIMP targets

From all noble elements, only argon and xenon are currently used as targets for dark matter detection. Neon has been suggested as a medium for low-energy neutrino detection, and could potentially be employed in the search for WIMPs [32]. In their liquid phase, noble elements are excellent media for building large, homogeneous, compact and self-shielding detectors. Liquid xenon (LXe) and liquid argon (LAr) are excellent scintillators and good ionizers in response to the passage of radiation. The simultaneous detection of ionization and scintillation signals allows to identify the primary particle interacting in the liquid, for the ratio of the two observables depends on dE/dx . In addition, the 3D position of an interaction can be determined with sub-mm (in the z-coordinate) to mm (in the x-y-coordinate) precisions in a time projection chamber (TPC). These features, together with the relative ease of scale-up to large detector masses, have contributed to make LXe and LAr powerful targets for WIMP searches [33, 34].

Table 4 summarizes the physical properties of argon and xenon. Their atomic number, density, boiling point temperature, dielectric constant, abundance in the atmosphere and intrinsic radioactive isotopes determine practical aspects of a dark matter detector. Xenon is heavier and its high liquid density helps to design a compact detector geometry with efficient self-shielding. Its fraction in the atmosphere is very low,

making it more expensive than natural argon. Xenon does not contain radioactive isotopes, apart from the double beta emitter ^{136}Xe , with a half-life recently measured to be $(2.165 \pm 0.016 \pm 0.059) \times 10^{21}$ yr [35].

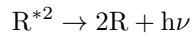
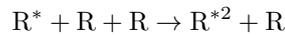
Property [unit]	Xe	Ar
Atomic number	54	18
Mean atomic weight	131.3	40.0
Boiling point T_b at 1 atm [K]	165.0	87.3
Melting point T_m at 1 atm [K]	161.4	83.8
Gas density at 1 atm & 298 K [g/l]	5.40	1.63
Gas density at 1 atm & T_b [g/l]	9.99	5.77
Liquid density at T_b [g/cm ³]	2.94	1.40
Volume ratio	526	795
Dielectric constant of liquid	1.95	1.51
Volume fraction in Earth's atmosphere [ppm]	0.09	9340
Radioactive isotopes	^{136}Xe , $T_{1/2} = 2.16 \times 10^{21}$ yr	^{39}Ar , $T_{1/2} = 269$ yr

Table 1: Physical properties, volume fraction in the atmosphere and radioactive isotopes of the noble elements xenon and argon.

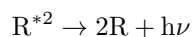
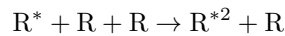
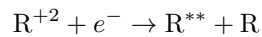
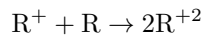
Atmospheric argon contains the radioactive ^{39}Ar , with a measured ratio of ^{39}Ar to ^{40}Ar of 8.1×10^{-16} g/g, resulting in a specific activity of ^{39}Ar of 1 Bq/kg [36]. Its production by cosmic ray induced reactions is dominated by the process $^{40}\text{Ar}(n,2n)^{39}\text{Ar}$, which has an energy threshold around 1 MeV. This increases the effective costs of argon for large dark matter detectors, since depletion in ^{39}Ar by isotopic separation or by extraction from underground wells is necessary. Depletion factors of larger than 100 have been achieved by using argon extracted from underground gas wells [37]. An anthropogenic radioactive isotope present in noble liquids extracted from air is ^{85}Kr . Currently achieved ^{nat}Kr -levels after purification using krypton-distillation columns are (1.0 ± 0.2) ppt [38] (with a detection limit by gas chromatography and mass spectrometry of 0.008 ppt), (3.5 ± 1.0) ppt [39] and < 2.7 ppt [40]. Levels of ~ 0.1 ppt will be necessary for an ultimate noble liquid dark matter detector [27].

The energy loss of an incident particle in noble liquids is shared between ionization, excitation and sub-excitation electrons liberated in the ionization process. The average energy loss in ionization is slightly larger than the ionization potential or the gap energy because it includes multiple ionization processes. Scintillation from noble liquids arises from excited atoms R^* and from ions R^+ , both being produced by ionizing radiation (see [33, 34] and references therein):

1.



2.



where $h\nu$ denotes the emitted vacuum-ultraviolet (VUV) photons with wavelength of 178 nm and 128 nm for LXe and LAr, respectively. $R^{**} \rightarrow R^* + \text{heat}$ corresponds to a non-radiative transition. In both processes, the excited dimer R^{*2} , at its lowest excited level, is de-excited to the dissociative ground state by the emission of a single UV photon. This comes from the large energy gap between the lowest excitation and the ground level, forbidding other decay channels such as non-radiative transitions. The scintillation light from pure liquid argon and xenon has two decay components due to de-excitation of singlet and triplet states of the excited dimer $R^{*2} \rightarrow 2R + h\nu$. The shorter decay shape is produced by the de-excitation of singlet states and the longer one by the de-excitation of triplet states. The differences of pulse shape between different type of particle interactions can be used to discriminate electronic from nuclear recoils, using the pulse shape discrimination (PSD) technique. It is particularly effective for liquid argon, given the large separation in time of the two decay components [41, 42].

In a given detection medium, the deposited energy for electronic and nuclear recoils can be expressed as (see [43] and references therein):

$$E_{er} = w(n_\gamma + n_{e^-}) \quad (2)$$

$$E_{nr} = w(n_\gamma + n_{e^-}) \frac{1}{\mathcal{L}} \quad (3)$$

where w is the average energy required for the production of a single photon or an electron, n_γ and n_{e^-} are the number of produced photons and electrons, respectively, and \mathcal{L} is the so-called Lindhard-factor. It quantifies the quenching of the observed signal for nuclear recoils, compared to the one for electronic recoils of the same energy. The w -value is ~ 14 eV and ~ 24 eV in LXe and LAr, respectively. The connection to actual signals observed in a dark matter detector, namely the prompt (S1) and proportional (S2) scintillations (the latter only in the case of dual-phase time projection chambers), is the following:

$$n_\gamma = \frac{S1}{\epsilon_1}, \quad n_{e^-} = \frac{S2}{\epsilon_2}, \quad (4)$$

where ϵ_1 is the photon detection efficiency (in phe/ γ) and ϵ_2 is the average number of photoelectrons (phe) per extracted electron into the vapour phase (in phe/ e^-), where 100% electron extraction efficiency is assumed.

The average number of photoelectrons per extracted electron can be measured *in situ*; it is for instance ~ 20 phe/ e^- in the XENON100 [44], and ~ 25 phe/ e^- in the LUX [45] xenon detectors. The photon detection efficiency is more difficult to determine directly, it is typically ~ 0.10 - 0.15 phe/ γ . Experiments thus usually report the light yield L_y (in phe/keV) for electronic recoils in a detector, which is measured at several energies using mono-energetic electron and gamma lines from a variety of sources. It includes the photon detection efficiency, geometrical effects and the quantum efficiency of the light sensors. In the past, the "standard candle" was taken as the 122 keV gamma line of ^{57}Co , most recently it shifted to the lower energy, 9.4 keV or the 32.1 keV, lines from ^{83m}Kr decays, for ^{83m}Kr can be used as an internal calibration source in both argon and xenon detectors [46, 47]. While for the 9.4 keV emission which follows the 31.2 keV line with a half-life of 154.4 ns, a time dependence of the scintillation signal is observed, the 32.1 keV transition shows no time dependence, and can safely be used as a "standard candle" [48]. The Noble Element Simulation Technique (NEST) considers all existing measurements of the light and charge yields for electronic and nuclear recoils (mostly in xenon, but also in argon) and it is used to simulate a given process in a single phase detector, or in a time projection chamber [49, 50].

In dark matter detectors using noble liquids, the energy of the nuclear recoil was traditionally established based on the observation of the primary scintillation signal alone. The scintillation light yield of nuclear recoils is different from the one produced by electron recoils of the same energy and the ratio at zero drift field, termed relative scintillation efficiency, \mathcal{L}_{eff} , is defined as follows:

$$\mathcal{L}_{\text{eff}}(E_{nr}) = \frac{S1}{L_y} \cdot \frac{1}{E_{nr}}, \quad (5)$$

where L_y is the light yield of electronic recoils at a given energy, as mentioned above. At non-zero drift field, a correction factor S_{er}/S_{nr} must be applied, where S_{er} , S_{nr} parametrize the suppression of the electronic and nuclear recoil signals due to the presence of the field.

For LXe, the relative scintillation efficiency of nuclear recoils has been measured down to 3 keV nuclear recoil energy (keV_{nr}) [51] at zero drift field. \mathcal{L}_{eff} is $\sim 9\%$, for nuclear recoils of 3 keV_{nr} and $\sim 14\%$ at 15 keV_{nr} . For higher energy nuclear recoils, the value is on average $\sim 19\%$. These measurements agree with indirect methods based on the data/MC comparison of nuclear recoil spectra in a given detector [52], and with a recent, in situ measurement by LUX, using a mono-energetic neutron beam and double-scatters to tag nuclear recoils [53]. The quantities S_{er} and S_{nr} depend on the applied electric field, but seem to be independent of energy. However more accurate, direct measurements are needed. In LAr, \mathcal{L}_{eff} at zero field has been measured down to 10 keV_{nr} and 16 keV_{nr} , respectively [54, 55]. An average value of 25% and 29% above an energy of 20 keV_{nr} and 16 keV_{nr} , is observed, with a turn up at lower recoil energies. A field dependance of up to 32% of the scintillation for nuclear recoils of energies between 10 keV_{nr} and 50 keV_{nr} has been observed [56], which increases with decreasing energy. Recently \mathcal{L}_{eff} in LAr was measured down to about 10 keV_{nr} , and no turn up at energies below 20 keV_{nr} is seen [57].

Nuclear recoils generated by WIMPs and fast, MeV neutrons have denser tracks, and thus greater electron-ion recombination than electron recoils. The collection of ionization electrons thus becomes more difficult for nuclear than for electron recoils. The ionization yield Q_y of nuclear recoils is defined as the number of observed electrons per unit recoil energy (e^-/keV_{nr}):

$$Q_y(E_{nr}) = \frac{S2}{\epsilon_2} \cdot \frac{1}{E_{nr}}. \quad (6)$$

In xenon, Q_y was measured for the first time by [58], as a function of external electric field and recoil energy. An increase in charge yield for low energy recoils was observed, explained by the lower recombination rate expected by the drop in electronic stopping power at low energies. This behaviour, although theoretically not fully understood, allows the observation of Xe nuclear recoils down to a few keV_{nr} , improving the event rate and the sensitivity for WIMP detection. Indirect measurements, obtained from a comparison of data and Monte Carlo simulations in a given detector down to 3 keV_{nr} [52], agree with previous data [59] and with the model by [60]. The ionization yield of nuclear recoils in LAr has been first measured by [61, 62] and recently by the SCENE collaboration [57, 63]. It also shows significantly less yield than the one from electronic recoils and an increase in the yield for lower recoil energies. In addition, an increase in the charge yield is observed for larger drift fields [57, 63].

For electronic recoils, the light yield in LXe was measured down to 1.5 keV recoils, with [48] and without [64] an applied drift field. At zero field, a reduced scintillation yield is observed below 10 keV, dropping to $\sim 40\%$ of its value at higher energies. With an applied field of 450 V/cm, a reduction of the scintillation output to about 75% relative to the value at zero field is observed. These measurement are particularly relevant for axion and axion-like-particle searches with liquid xenon detectors [65, 66], as well as for searches of other dark matter candidates that might interact with electrons, and of neutrino-electron scattering [27].

4.1. The single and dual-phase detector technology

In single-phase liquid argon or xenon dark matter detectors, the experimental strategy is to use the self-shielding of the liquid in order to achieve an effectively background-free inner volume, coupled to pulse shape discrimination in the case of argon. The self-shielding works better for the gamma-, than for the neutron background, given the differences in their mean free paths. The position of an interaction can be reconstructed using the observed light pattern in the photodetectors, which are usually mounted on the inner detector surface. The position resolution will depend on the size of the photodetectors, as well as on the overall light yield. The main advantage of these detectors is their simplicity compared to time projection chambers. Since no electrons are drifted, the need for a high-voltage and a cathode-anode-grid system falls away. It goes at the cost of a large amount of expensive (in the case of xenon, and of argon depleted in ^{39}Ar) cryogenic liquid which is used as shield.

A disadvantage, in particular for xenon detectors, rests in the fact that less information per event becomes available. In liquid xenon, there is no well-defined separation between electron and nuclear recoils based on

the pulse shape of events, since the mean lifetime of the singlet and triplet states are not well separated in time (3 ns versus 27 ns). These detectors thus rely on the absolute suppression of both external and internal electronic recoil sources. In LAr, the decay times of the singlet and triplet state differ by two orders of magnitude, being $\tau_s = 7$ ns and $\tau_t = 1.6$ μ s, respectively. The ratio between the emission intensities of the singlet/triplet states depends on the deposited energy per unit path length, dE/dx . It has been measured to be about 0.3 for gammas, in the range of 1.3-3 for alphas and about 3 for argon ion recoils [41, 42, 67]. The difference in the pulse shapes is employed to distinguish between electronic and nuclear recoils, where a discrimination power of $\sim 10^6$ has been achieved for nuclear recoil energies above ~ 50 keV [42]. Because of the shorter wavelength of the scintillation light in LAr (128 nm), the inner detector surfaces and the PMT windows must be coated with a wavelength shifter, such as for instance tetra phenyl butadiene (TPB), which shifts the wavelength of the light to about 442 nm [68]. One must ensure an optimal efficiency of the wavelength shifter, and its long-term stability in time in a cold, LAr environment.

Two-phase detectors rely on the time projection chamber technique. An interaction within the so-called active volume of the detector will create ionization electrons and prompt scintillation photons, and both signals are detected. The electrons drift in the pure liquid under the influence of an external electric field, are then accelerated by a stronger field and extracted into the vapour phase above the liquid, where they generate proportional scintillation, or electroluminescence. Two arrays of photosensors, one in the liquid and one in the gas, detect the prompt scintillation (S1) and the delayed, proportional scintillation signal (S2). The array immersed in the liquid collects the majority of the prompt signal, which is totally reflected at the liquid-gas interface. The ratio of the two signals is different for nuclear recoils created by WIMP or neutron interactions, and electronic recoils produced by β and γ -rays, providing the basis for background discrimination. Since electron diffusion in the ultra-pure liquid is small, the proportional scintillation photons carry the $x-y$ information of the interaction site. With the z -information from the drift time measurement, the TPC yields a three-dimensional event localization, enabling to reject the majority of the background via fiducial volume cuts.

4.2. Current xenon experiments

The most stringent limits for spin-independent WIMP-nucleon couplings to date come from the dual-phase LXe TPCs ZEPLIN-III [69, 70], XENON10 [71, 72], XENON100 [73, 74, 75] and LUX [39], where XENON100 and LUX are currently running experiments. XENON100, a 161 kg LXe TPC, is operated in the interferometer tunnel at LNGS in Italy. It employs two arrays of low-radioactivity, UV-sensitive photomultipliers (PMTs) to detect the prompt and proportional light signals induced by particles interacting in the xenon volume, containing 62 kg of ultra-pure liquid xenon. The remaining 99 kg of LXe act as an active veto shield against background events. The instrument is described in [74], the analysis procedure is detailed in [76]. Using 13 months of data taken during 2011 and 2012, with an exposure of 224.6 live days \times 34 kg, XENON100 had reached its initial aim to probe spin-independent WIMP-nucleon cross sections down to 2×10^{-45} cm² at a 55 GeV WIMP mass [75]. New limits on WIMP-nucleon spin-dependent couplings were also derived [77], yielding the world's best sensitivity on WIMP-neutron couplings. After a further distillation run to reduce the Kr concentration to (0.95 ± 0.16) ppt of ^{nat}Kr in LXe in the latest XENON100 run [38], a new dark matter run started in 2013, and lasted for 150 days. The blind analysis of this data is in progress.

The Large Underground Xenon (LUX) experiment is a 370 kg (250 kg) total (active) mass LXe TPC in a water Cherenkov shield at the Sanford Underground Research Facility (SURF) in Lead, South Dakota, USA [78]. The TPC is 47 cm in diameter and 48 cm in height, the S1 and S2 signals are detected via two arrays of 61 PMTs, one in the liquid and one in the gas region. A first science run lasted from April to August 2013, for 85.3 live-days. A non-blind analysis was performed using a fiducial volume of 118 kg and a software imposed energy threshold of 3 keV_{nr}. The reached 90% upper C.L. cross section for spin-independent WIMP-nucleon couplings has a minimum of 7.6×10^{-46} cm² at a WIMP mass of 33 GeV/ c^2 , thus confirming and improving upon the XENON100 results. LUX plans to continue operations at SURF in 2014 and 2015, and to reach its sensitivity goal with a blinded 300 live-day WIMP search [39].

The XMASS collaboration operates a large, single-phase LXe detector with 835 kg in the sensitive region, at the Kamioka Observatory in the Kamioka mine in Japan [79]. The inner detector is equipped with 642

hexagonal PMTs in an almost spherical shape, contained in a copper vessel filled with LXe. The outer detector, used as an active shield for cosmic muons, is a cylindrical water tank, 10 m in height and 10 m in diameter, equipped with 70 20-inch PMTs. XMASS recently published a result for low-mass WIMPs [80] as well as limits on inelastic WIMP- ^{129}Xe scatters [81]. The collaboration is currently operating a refurbished detector with reduced background levels, with new results expected for 2014.

PandaX is a dual-phase xenon TPC at the Jinping laboratory in Sichuan, China, operated in a conventional low-background shield [82]. In its first stage, it plans to increase the fiducial mass from 25 kg to 300 kg of xenon, with a total target mass of about 500 kg. The active xenon region is viewed by 150 1-inch R8520 PMTs on the top, and 40 3-inch R11410-10 PMTs on the bottom array. PandaX completed two engineering runs in 2013, and is currently preparing the first physics run with 450 kg of xenon in the system [83].

XENON1T, the next step of the XENON program, is a dual-phase xenon TPC with total (active) mass of 3.3 t (~ 2 t). The active LXe volume will be viewed by 248 Hamamatsu R11410-21 3-inch PMTs, arranged in two arrays. The PMTs, with an average quantum efficiency of 36% at 175 nm, were extensively tested for their long-term stability in liquid xenon [84]. The underground construction of XENON1T started in Hall B of LNGS in the fall of 2013, completion and commissioning are expected for early and mid 2015, respectively. With an aimed background which is two orders of magnitude below the one from XENON100, a sensitivity to spin-independent cross sections of $2 \times 10^{-47} \text{ cm}^2$ is expected after two years of continuous operation underground.

4.3. Current argon experiments

DarkSide-50 [85] is a dual-phase argon detector with 50 kg (33 kg) active (fiducial) mass, viewed by 38 Hamamatsu R11065 3-inch PMTs. The TPC is surrounded by a 30 t borated-liquid scintillator neutron veto and both detectors are deployed in the Borexino Counting Test Facility (CTF), a 1 kton water Cherenkov shield in Hall C of LNGS. The collaboration has recently presented first results from a run with natural argon, demonstrating a light yield of 8 phe/keV at 41.5 keV and zero field, and an electron-lifetime >5 ms for a maximum drift time of 370 μs . A background free exposure of 280 kg day allowed to prove the efficiency of the PSD, predicting no background in 2.6 y of a run with argon depleted in the radioactive isotope ^{39}Ar . The projected sensitivity using the measured PSD performance, an energy threshold of 35 keV $_{nr}$ and a data taking period of 3 years is $\sim 10^{-45} \text{ cm}^2$ for a 100 GeV WIMP [86].

The ArDM experiment operates a ton-scale dual-phase Ar TPC at the Canfranc Underground Laboratory in Spain [87]. The active detector volume, containing 850 kg of LAr, is viewed by two arrays of 12 8-inch PMTs arranged in a honeycomb pattern. TPB is deposited on the PMT windows and on a Tetratex reflector installed on the field shaping rings. The detector and its infrastructure were installed underground successfully, and first data acquired with the detector filled with pure Ar gas at room temperature has allowed the assessment of the light detection system's performance [88]. Commissioning with liquid argon is expected for mid 2014, and first results are expected for 2015.

The MiniCLEAN [89] and DEAP-3600 [90] experiments are single-phase LAr detectors operated at SNOLab in Sudbury, Canada. MiniCLEAN will operate 500 kg of LAr in an inner stainless steel vessel of about 64-inch in diameter, contained in a vacuum cryostat. The assembly is located inside a large water shield operated as muon veto. The liquid argon is viewed by 92 optical modules, containing each one 8-inch Hamamatsu R5912-02Mod PMT, coupled to a light guide and an acrylic plug at the end. The plug front surfaces, coated with TPB, form the 92-sided sphere that contains the cryogenic volume. The MiniCLEAN detector is nearing completion underground, cooling with cold gas and liquidation of argon are scheduled to start in summer 2014 [89]. The DEAP-3600 detector will operate 3600 kg LAr (with 1000 kg fiducial mass), in a large acrylic vessel with an inner radius of 85 cm. The LAr is viewed by 255 8-inch PMTs through 50 cm light guides. These provide thermal insulation between the cryogenic acrylic vessel and the PMTs, as well as a shield against neutrons. The inner detector is housed in a spherical stainless steel vessel immersed in an 8 m diameter water tank [90]. The detector is under construction at SNOLab and first results are expected within one year. The sensitivity aim with argon depleted in ^{39}Ar is $<1 \times 10^{-46} \text{ cm}^2$ at a WIMP mass of 100 GeV.

4.4. Future projects and complementarity

Existing results and projected sensitivities for the spin-independent WIMP-nucleon interactions as a function of the WIMP mass are summarized in Figure 3, adapted from [91]. In spite of observed anomalies in a handful of experiments, that could be interpreted as due to WIMPs, albeit not consistently, we have no convincing evidence of a direct detection signal induced by galactic dark matter. Considering LUX’s lack of a signal in 85.3 live-days \times 118 kg of liquid xenon target, excluding \sim 33 GeV WIMPs with interaction strengths above $7.6\times 10^{-46}\text{cm}^2$, it becomes clear that, at the minimum, ton-scale experiments are required for a discovery above the 5-sigma confidence level (unless the WIMP is lighter than \sim 10 GeV, where larger cross sections are feasible). Several large-scale direct detection experiments are in their planning phase and will start science runs within this decade.

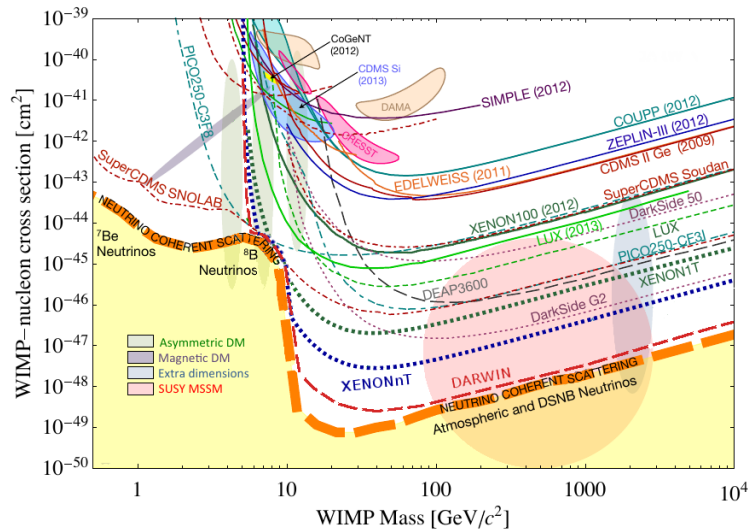


Figure 3: Summary for spin-independent WIMP-nucleon scattering results. Existing limits from the noble gas dark matter experiments ZEPLIN-III [69], XENON10 [71], XENON100 [75], and LUX [39], along with projections for DarkSide-50 [85], LUX [39], DEAP3600 [90], XENON1T, DarkSide G2, XENONnT (similar sensitivity as the LZ project [92], see text) and DARWIN [93] are shown. DARWIN is designed to probe the entire parameter region for WIMP masses above \sim 6 GeV/ c^2 , until the neutrino background (yellow region) will start to dominate the recoil spectrum. Experiments based on the mK cryogenic technique such as SuperCDMS [94] and EURECA [95] have access to lower WIMP masses. Figure adapted from [91].

The next phase in the LUX program, LUX-ZEPLIN (LZ), foresees a 7 t LXe detector in the same SURF infrastructure, with an additional scintillator veto to suppress the neutron background. Construction is expected to start in 2014, and operation in 2016, with the goal of reaching a sensitivity of $2\times 10^{-48}\text{cm}^2$ after three years of data taking [92]. The upgrade of XENON1T, XENONnT, is to increase the sensitivity by another order of magnitude, thus also reaching $2\times 10^{-48}\text{cm}^2$. While much of the XENON1T infrastructure will be reused, the inner detector will be designed and constructed once XENON1T is taking science data, with planned operation between 2018-2021. The XMASS collaboration plans a 5 t (1 t fiducial) single-phase detector after its current phase, with greatly reduced backgrounds and an aimed sensitivity of $\sim 10^{-46}\text{cm}^2$. In its second stage, PandaX will operate a total of 1.5 t LXe as WIMP target, with \sim 1 t xenon in the fiducial volume. All sub-systems of the existing experiment, with the exception of the central TPC, are designed to accommodate the larger target mass [83]. The DarkSide collaboration plans a 5 t LAr dual-phase detector, with 3.3 t as active target mass, in the existing neutron and muon veto at LNGS. The aimed sensitivity is 10^{-47}cm^2 [96].

Dark matter WImp search with Noble liquids (DARWIN) is an initiative to build an ultimate, multi-ton dark matter detector at LNGS [97, 93]. Its primary goal is to probe the spin-independent WIMP-nucleon cross section down to the 10^{-49}cm^2 region for \sim 50 GeV/ c^2 WIMPs, as shown in Figure 3. It would thus explore the experimentally accessible parameter space, which will be finally limited by irreducible neutrino backgrounds. Should WIMPs be discovered by an existing or near-future experiment, DARWIN will measure WIMP-induced nuclear recoil spectra with high-statistics, constraining the mass and the scattering cross section of the dark matter particle [98, 99]. Other physics goals of DARWIN are the first real-time detection of solar pp-neutrinos with high statistics and the search for the neutrinoless double beta decay [27]. The latter would establish whether the neutrino is its own anti-particle, and can be detected via ^{136}Xe , which has a natural abundance of 8.9% in xenon.

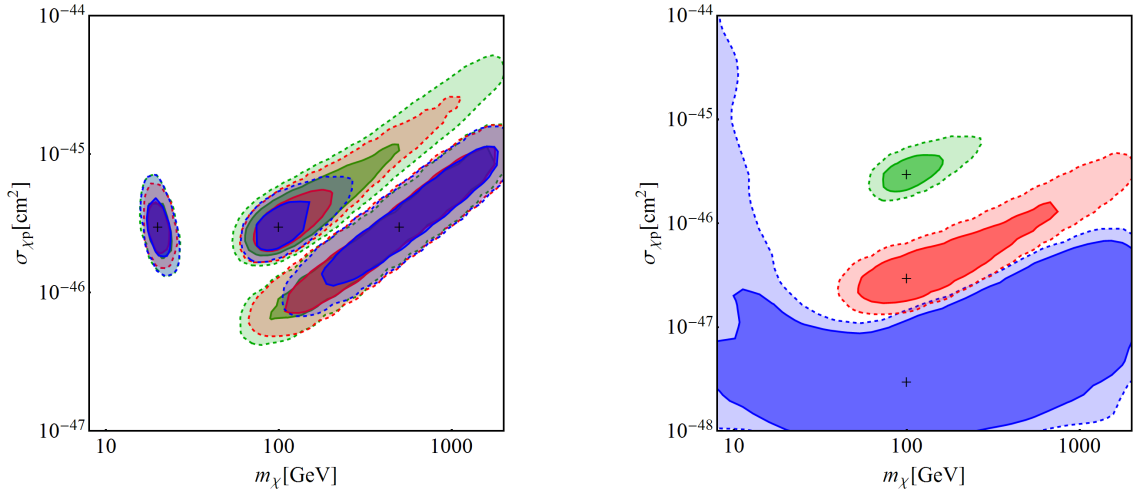


Figure 4: The $1\text{-}\sigma$ and $2\text{-}\sigma$ credible regions of the marginal posterior probabilities for simulations of WIMPs of various masses and cross sections demonstrate how well the WIMP parameters can be reconstructed for different exposures of a LXe or LAr detector. The ‘+’ indicates the simulated model. (Left) Exposures of $10\text{ t}\times\text{yr}$ xenon (green), $20\text{ t}\times\text{yr}$ LXe (red), and $10\text{ t}\times\text{yr}$ LXe plus $20\text{ t}\times\text{yr}$ LAr (blue). (Right) $10\text{ t}\times\text{yr}$ LXe plus $20\text{ t}\times\text{yr}$ LAr exposure for cross sections of $3 \times 10^{-46}\text{ cm}^2$ (green), $3 \times 10^{-47}\text{ cm}^2$ (red) and $3 \times 10^{-48}\text{ cm}^2$ (blue). Figure from [99].

As soon as direct evidence for a dark matter signal has been established with so-called discovery experiments, the efforts will shift towards measuring the mass and cross section of the dark matter particle. This information is complementary to the one provided by indirect detection experiments such as IceCube, AMS and CTA, and by dark matter searches with ATLAS and CMS at the LHC. Figure 4.4 (left) displays the capability of a large LXe/LAr detector to reconstruct the WIMP mass and cross section for various masses and a hypothetical WIMP-nucleon cross section of $3 \times 10^{-46}\text{ cm}^2$ [99]. Exposures of $10\text{ t}\times\text{yr}$ and $20\text{ t}\times\text{yr}$ using a LXe target only, as well as a combined exposure of $10\text{ t}\times\text{yr}$ LXe and of $20\text{ t}\times\text{yr}$ LAr, were assumed. The right side of the same Figure shows the reconstructed mass and cross sections for a $100\text{ GeV}/c^2$ WIMP, and several cross sections, using the combined exposure of $10\text{ t}\times\text{yr}$ xenon and $20\text{ t}\times\text{yr}$ argon. The study assumes nuclear recoil energy thresholds of $6.6\text{ keV}_{\text{nr}}$ and $20\text{ keV}_{\text{nr}}$ in xenon and argon, respectively. The uncertainties on the dark matter halo parameters $\rho_0=(0.3\pm 0.1)\text{ GeV}/\text{cm}^2$, $v_0=(220\pm 20)\text{ km}/\text{s}$ and $v_{esc}=(544\pm 40)\text{ km}/\text{s}$ are taken into account.

5. Summary and Outlook

Dark matter detectors based on liquified noble gases have matured into a robust technology for detecting the minuscule energy deposited into a medium when a WIMP scatters off an atomic nucleus in the target. They have demonstrated the lowest backgrounds reached up to now in any direct detection experiment, and their scale up to large, homogeneous target masses is rather straightforward. While detectors currently in operation have reached background levels as low as a few events/(keV t d) in the dark matter region of interest, before discrimination of electronic and nuclear recoils, detectors under commissioning and/or construction will improve these absolute backgrounds by a few orders of magnitude, until the irreducible neutrino background will start to dominate the recoil spectra. These ton- and multi-ton scale noble liquid detectors should reach sensitivities that will allow them to probe the entire experimentally accessible region for WIMP masses above $\sim 6\text{ GeV}$. Figure 5 shows the evolution of upper limits on the spin-independent cross section as a function of time, together with latest projections for the future.

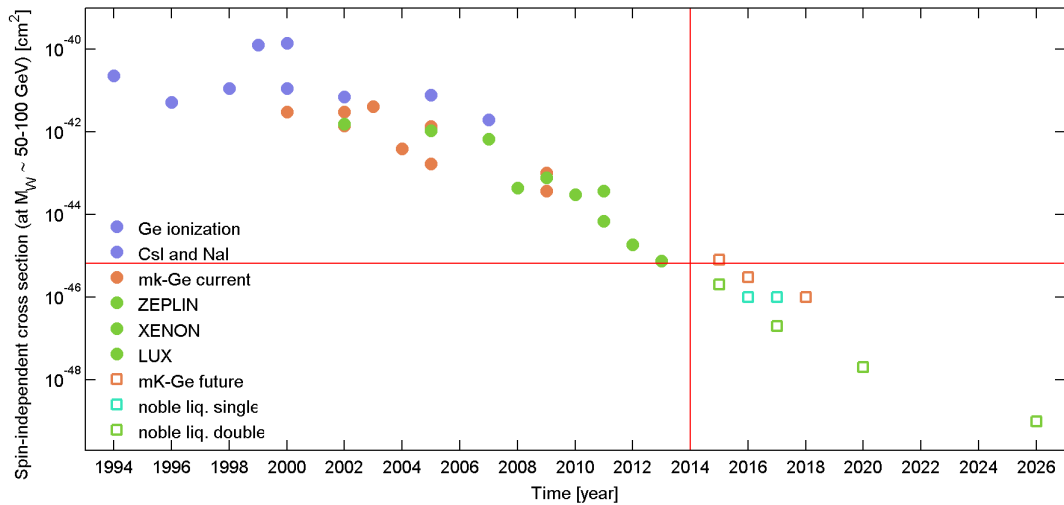


Figure 5: Existing upper limits on spin-independent WIMP-nucleon cross sections (for WIMP masses around 50–100 GeV) from various direct detection techniques (filled circles), along with projections for the future (open squares), as a function time (Figure updated from [100]).

Acknowledgments

This work is supported by the University of Zurich, by the Swiss National Foundation (SNF) Grant No 200020-149256 and by the FP7 Marie Curie-ITN action PITN-GA-2011-289442 *Invisibles*.

References

- [1] P. Ade, et al., Planck 2013 results. XVI. Cosmological parameters [arXiv:1303.5076](#).
- [2] B. W. Lee, S. Weinberg, Cosmological Lower Bound on Heavy Neutrino Masses, *Phys.Rev.Lett.* 39 (1977) 165–168. [doi:10.1103/PhysRevLett.39.165](#).
- [3] G. Jungman, M. Kamionkowski, K. Griest, Supersymmetric dark matter, *Phys.Rept.* 267 (1996) 195–373. [arXiv:hep-ph/9506380](#), [doi:10.1016/0370-1573\(95\)00058-5](#).
- [4] D. Hooper, S. Profumo, Dark matter and collider phenomenology of universal extra dimensions, *Phys.Rept.* 453 (2007) 29–115. [arXiv:hep-ph/0701197](#), [doi:10.1016/j.physrep.2007.09.003](#).
- [5] G. Bertone, D. Hooper, J. Silk, Particle dark matter: Evidence, candidates and constraints, *Phys.Rept.* 405 (2005) 279–390. [arXiv:hep-ph/0404175](#), [doi:10.1016/j.physrep.2004.08.031](#).
- [6] G. Raffelt, Axions, *Space Sci.Rev.* 100 (2002) 153–158. [doi:10.1023/A:1015822212542](#).
- [7] K. Baker, G. Cantatore, S. Cetin, M. Davenport, K. Desch, et al., The quest for axions and other new light particles, *Annalen Phys.* 525 (2013) A93–A99. [arXiv:1306.2841](#), [doi:10.1002/andp.201300727](#).
- [8] G. Rybka, Direct Detection Searches for Axion Dark Matter, *Phys.Dark Univ.* 4 (2014) 14–16. [doi:10.1016/j.dark.2014.05.003](#).
- [9] M. W. Goodman, E. Witten, Detectability of Certain Dark Matter Candidates, *Phys.Rev.* D31 (1985) 3059. [doi:10.1103/PhysRevD.31.3059](#).
- [10] J. Lewin, P. Smith, Review of mathematics, numerical factors, and corrections for dark matter experiments based on elastic nuclear recoil, *Astropart.Phys.* 6 (1996) 87–112. [doi:10.1016/S0927-6505\(96\)00047-3](#).
- [11] A. M. Green, Astrophysical uncertainties on direct detection experiments, *Mod.Phys.Lett.* A27 (2012) 1230004. [arXiv:1112.0524](#), [doi:10.1142/S0217732312300042](#).
- [12] M. C. Smith, et al., The RAVE Survey: Constraining the Local Galactic Escape Speed, *Mon. Not. Roy. Astron. Soc.* 379 (2007) 755–772. [arXiv:astro-ph/0611671](#), [doi:10.1111/j.1365-2966.2007.11964.x](#).
- [13] M. Vogelsberger, A. Helmi, V. Springel, S. D. White, J. Wang, et al., Phase-space structure in the local dark matter distribution and its signature in direct detection experiments, *Mon.Not.Roy.Astron.Soc.* 395 (2009) 797–811. [arXiv:0812.0362](#), [doi:10.1111/j.1365-2966.2009.14630.x](#).
- [14] J. Read, The Local Dark Matter Density [arXiv:1404.1938](#).
- [15] J. Menendez, D. Gazit, A. Schwenk, Spin-dependent WIMP scattering off nuclei, *Phys.Rev.* D86 (2012) 103511. [arXiv:1208.1094](#), [doi:10.1103/PhysRevD.86.103511](#).

- [16] P. Klos, J. Menendez, D. Gazit, A. Schwenk, Large-scale nuclear structure calculations for spin-dependent WIMP scattering with chiral effective field theory currents, *Physical Review D* 88, 083516. [arXiv:1304.7684](#).
- [17] J. Fan, M. Reece, L.-T. Wang, Non-relativistic effective theory of dark matter direct detection, *JCAP* 1011 (2010) 042. [arXiv:1008.1591](#), [doi:10.1088/1475-7516/2010/11/042](#).
- [18] A. L. Fitzpatrick, W. Haxton, E. Katz, N. Lubbers, Y. Xu, The Effective Field Theory of Dark Matter Direct Detection, *JCAP* 1302 (2013) 004. [arXiv:1203.3542](#), [doi:10.1088/1475-7516/2013/02/004](#).
- [19] R. J. Hill, M. P. Solon, WIMP-nucleon scattering with heavy WIMP effective theory, *Phys.Rev.Lett.* 112 (2014) 211602. [arXiv:1309.4092](#), [doi:10.1103/PhysRevLett.112.211602](#).
- [20] N. Anand, A. L. Fitzpatrick, W. Haxton, Model-independent WIMP Scattering Responses and Event Rates: A Mathematica Package for Experimental Analysis, *Phys.Rev.* C89 (2014) 065501. [arXiv:1308.6288](#), [doi:10.1103/PhysRevC.89.065501](#).
- [21] L. Baudis, G. Kessler, P. Klos, R. Lang, J. Menendez, et al., Signatures of Dark Matter Scattering Inelastically Off Nuclei, *Phys.Rev.* D88 (2013) 115014. [arXiv:1309.0825](#), [doi:10.1103/PhysRevD.88.115014](#).
- [22] G. Heusser, Low-radioactivity background techniques, *Ann.Rev.Nucl.Part.Sci.* 45 (1995) 543–590. [doi:10.1146/annurev.ns.45.120195.002551](#).
- [23] M. Haffke, L. Baudis, T. Bruch, A. Ferella, T. Marrodan Undagoitia, et al., Background Measurements in the Gran Sasso Underground Laboratory, *Nucl.Instrum.Meth.* A643 (2011) 36–41. [arXiv:1101.5298](#), [doi:10.1016/j.nima.2011.04.027](#).
- [24] M. Selvi, Study of the performances of the shield and muon veto of the XENON1T experiment, *PoS IDM2010* (2011) 053.
- [25] L. Baudis, A. Ferella, A. Askin, J. Angle, E. Aprile, et al., Gator: a low-background counting facility at the Gran Sasso Underground Laboratory, *JINST* 6 (2011) P08010. [arXiv:1103.2125](#), [doi:10.1088/1748-0221/6/08/P08010](#).
- [26] D.-M. Mei, C. Zhang, A. Hime, Evaluation of (alpha,n) Induced Neutrons as a Background for Dark Matter Experiments, *Nucl.Instrum.Meth.* A606 (2009) 651–660. [arXiv:0812.4307](#), [doi:10.1016/j.nima.2009.04.032](#).
- [27] L. Baudis, A. Ferella, A. Kish, A. Manalaysay, T. M. Undagoitia, et al., Neutrino physics with multi-ton scale liquid xenon detectors, *JCAP* 01 (2014) 044. [arXiv:1309.7024](#), [doi:10.1088/1475-7516/2014/01/044](#).
- [28] L. E. Strigari, Neutrino Coherent Scattering Rates at Direct Dark Matter Detectors, *New J.Phys.* 11 (2009) 105011. [arXiv:0903.3630](#), [doi:10.1088/1367-2630/11/10/105011](#).
- [29] A. Gutlein, C. Ciemiak, F. von Feilitzsch, N. Haag, M. Hofmann, et al., Solar and atmospheric neutrinos: Background sources for the direct dark matter search, *Astropart.Phys.* 34 (2010) 90–96. [arXiv:1003.5530](#), [doi:10.1016/j.astropartphys.2010.06.002](#).
- [30] J. Billard, L. Strigari, E. Figueroa-Feliciano, Implication of neutrino backgrounds on the reach of next generation dark matter direct detection experiments, *Phys.Rev.* D89 (2014) 023524. [arXiv:1307.5458](#).
- [31] A. Anderson, J. Conrad, E. Figueroa-Feliciano, K. Scholberg, J. Spitz, Coherent Neutrino Scattering in Dark Matter Detectors, *Phys.Rev.* D84 (2011) 013008. [arXiv:1103.4894](#), [doi:10.1103/PhysRevD.84.013008](#).
- [32] W. Lippincott, et al., Scintillation yield and time dependence from electronic and nuclear recoils in liquid neon, *Phys.Rev.* C86 (2012) 015807. [arXiv:1111.3260](#), [doi:10.1103/PhysRevC.86.015807](#).
- [33] E. Aprile, L. Baudis, Liquid noble gases, In *Bertone, G. (ed.): Particle dark matter* 413–436.
- [34] V. Chepel, H. Araujo, Liquid noble gas detectors for low energy particle physics, *JINST* 8 (2013) R04001. [arXiv:1207.2292](#), [doi:10.1088/1748-0221/8/04/R04001](#).
- [35] J. Albert, et al., An improved measurement of the $2\nu\beta\beta$ half-life of Xe-136 with EXO-200, *Phys.Rev.* C89 (2014) 015502. [arXiv:1306.6106](#), [doi:10.1103/PhysRevC.89.015502](#).
- [36] P. Benetti, et al., Measurement of the specific activity of ar-39 in natural argon, *Nucl.Instrum.Meth.* A574 (2007) 83–88. [arXiv:astro-ph/0603131](#), [doi:10.1016/j.nima.2007.01.106](#).
- [37] H. O. Back, F. Calaprice, C. Condon, E. de Haas, R. Ford, et al., First Large Scale Production of Low Radioactivity Argon From Underground Sources [arXiv:1204.6024](#).
- [38] S. Lindemann, H. Simgen, Krypton assay in xenon at the ppq level using a gas chromatographic system and mass spectrometer, *Eur.Phys.J.* C74 (2014) 2746. [arXiv:1308.4806](#), [doi:10.1140/epjc/s10052-014-2746-1](#).
- [39] D. Akerib, et al., First results from the LUX dark matter experiment at the Sanford Underground Research Facility [arXiv:1310.8214](#).
- [40] K. Abe, K. Hieda, K. Hiraide, S. Hirano, Y. Kishimoto, et al., XMASS detector, *Nucl.Instrum.Meth.* A716 (2013) 78–85. [arXiv:1301.2815](#), [doi:10.1016/j.nima.2013.03.059](#).
- [41] A. Hitachi, T. Takahashi, N. Funayama, K. Masuda, J. Kikuchi, et al., Effect of ionization density on the time dependence of luminescence from liquid argon and xenon, *Phys.Rev.* B27 (1983) 5279–5285. [doi:10.1103/PhysRevB.27.5279](#).
- [42] W. Lippincott, K. Coakley, D. Gastler, A. Hime, E. Kearns, et al., Scintillation time dependence and pulse shape discrimination in liquid argon, *Phys.Rev.* C78 (2008) 035801. [arXiv:0801.1531](#), [doi:10.1103/PhysRevC.81.039901](#), [10.1103/PhysRevC.78.035801](#).
- [43] P. Sorensen, C. E. Dahl, Nuclear recoil energy scale in liquid xenon with application to the direct detection of dark matter, *Phys.Rev.* D83 (2011) 063501. [arXiv:1101.6080](#), [doi:10.1103/PhysRevD.83.063501](#).
- [44] E. Aprile, et al., Observation and applications of single-electron charge signals in the XENON100 experiment, *J.Phys.* G41 (2014) 035201. [arXiv:1311.1088](#), [doi:10.1088/0954-3899/41/3/035201](#).
- [45] M. Szydagis, et al., A Detailed Look at the First Results from the Large Underground Xenon (LUX) Dark Matter Experiment [arXiv:1402.3731](#).
- [46] A. Manalaysay, T. Undagoitia, A. Askin, L. Baudis, A. Behrens, et al., Spatially uniform calibration of a liquid xenon detector at low energies using ^{83m}Kr , *Rev.Sci.Instrum.* 81 (2010) 073303. [arXiv:0908.0616](#), [doi:10.1063/1.3436636](#).
- [47] L. Kastens, S. Cahn, A. Manzur, D. McKinsey, Calibration of a Liquid Xenon Detector with ^{83m}Kr , *Phys.Rev.* C80

- (2009) 045809. [arXiv:0905.1766](#), [doi:10.1103/PhysRevC.80.045809](#).
- [48] L. Baudis, H. Dujmovic, C. Geis, A. James, A. Kish, et al., Response of liquid xenon to Compton electrons down to 1.5 keV, *Phys.Rev. D87* (11) (2013) 115015. [arXiv:1303.6891](#), [doi:10.1103/PhysRevD.87.115015](#).
- [49] M. Szydagis, A. Fyhrie, D. Thorngren, M. Tripathi, Enhancement of NEST Capabilities for Simulating Low-Energy Recoils in Liquid Xenon, *JINST* 8 (2013) C10003. [arXiv:1307.6601](#), [doi:10.1088/1748-0221/8/10/C10003](#).
- [50] M. Szydagis, N. Barry, K. Kazkaz, J. Mock, D. Stolp, et al., NEST: A Comprehensive Model for Scintillation Yield in Liquid Xenon, *JINST* 6 (2011) P10002. [arXiv:1106.1613](#), [doi:10.1088/1748-0221/6/10/P10002](#).
- [51] G. Plante, E. Aprile, R. Budnik, B. Choi, K. Giboni, et al., New Measurement of the Scintillation Efficiency of Low-Energy Nuclear Recoils in Liquid Xenon, *Phys.Rev. C84* (2011) 045805. [arXiv:1104.2587](#), [doi:10.1103/PhysRevC.84.045805](#).
- [52] E. Aprile, et al., Response of the XENON100 Dark Matter Detector to Nuclear Recoils, *Phys.Rev. D88* (2013) 012006. [arXiv:1304.1427](#), [doi:10.1103/PhysRevD.88.012006](#).
- [53] C. Carmona, First dark matter results from the LUX experiment, Talk at DM 2014, UCLA.
- [54] D. Gastler, E. Kearns, A. Hime, L. Stonehill, S. Seibert, et al., Measurement of scintillation efficiency for nuclear recoils in liquid argon, *Phys.Rev. C85* (2012) 065811. [arXiv:1004.0373](#), [doi:10.1103/PhysRevC.85.065811](#).
- [55] C. Regenfuss, Y. Allkofer, C. Amsler, W. Creus, A. Ferella, et al., Study of nuclear recoils in liquid argon with monoenergetic neutrons, *J.Phys.Conf.Ser.* 375 (2012) 012019. [arXiv:1203.0849](#), [doi:10.1088/1742-6596/375/1/012019](#).
- [56] T. Alexander, et al., Observation of the Dependence of Scintillation from Nuclear Recoils in Liquid Argon on Drift Field, *Phys.Rev. D88* (2013) 092006. [arXiv:1306.5675](#), [doi:10.1103/PhysRevD.88.092006](#).
- [57] H. Lippincot, Response of liquid noble gases to nuclear recoils, Talk at the LHC results forum.
- [58] E. Aprile, et al., Simultaneous Measurement of Ionization and Scintillation from Nuclear Recoils in Liquid Xenon as Target for a Dark Matter Experiment, *Phys. Rev. Lett.* 97 (2006) 081302. [arXiv:astro-ph/0601552](#), [doi:10.1103/PhysRevLett.97.081302](#).
- [59] A. Manzur, A. Curioni, L. Kastens, D. McKinsey, K. Ni, et al., Scintillation efficiency and ionization yield of liquid xenon for mono-energetic nuclear recoils down to 4 keV, *Phys.Rev. C81* (2010) 025808. [arXiv:0909.1063](#), [doi:10.1103/PhysRevC.81.025808](#).
- [60] F. Bezrukov, F. Kahlhoefer, M. Lindner, Interplay between scintillation and ionization in liquid xenon Dark Matter searches, *Astropart.Phys.* 35 (2011) 119–127. [arXiv:1011.3990](#), [doi:10.1016/j.astropartphys.2011.06.008](#).
- [61] L. Grandi, WARP: an argon double phase technique for Dark Matter search, Ph.D. Thesis, University of Pavia.
- [62] P. Benetti, et al., First results from a dark matter search with liquid argon at 87-K in the Gran Sasso underground laboratory, *Astropart. Phys.* 28 (2008) 495–507. [arXiv:astro-ph/0701286](#), [doi:10.1016/j.astropartphys.2007.08.002](#).
- [63] H. Cao, et al., Measurement of Scintillation and Ionization Yield and Scintillation Pulse Shape from Nuclear Recoils in Liquid Argon [arXiv:1406.4825](#).
- [64] E. Aprile, R. Budnik, B. Choi, H. Contreras, K. Giboni, et al., Measurement of the Scintillation Yield of Low-Energy Electrons in Liquid Xenon, *Phys.Rev. D86* (2012) 112004. [arXiv:1209.3658](#), [doi:10.1103/PhysRevD.86.112004](#).
- [65] K. Abe, K. Hieda, K. Hiraide, S. Hirano, Y. Kishimoto, et al., Search for solar axions in XMASS, a large liquid-xenon detector, *Phys. Lett. B* 724 (2013) 46–50. [arXiv:1212.6153](#), [doi:10.1016/j.physletb.2013.05.060](#).
- [66] E. Aprile, F. Agostini, M. Alfonsi, K. Arisaka, F. Arneodo, et al., First Axion Results from the XENON100 Experiment [arXiv:1404.1455](#).
- [67] P. Peiffer, T. Pollmann, S. Schonert, A. Smolnikov, S. Vasiliev, Pulse shape analysis of scintillation signals from pure and xenon-doped liquid argon for radioactive background identification, *JINST* 3 (2008) P08007. [doi:10.1088/1748-0221/3/08/P08007](#).
- [68] C. Amsler, et al., Luminescence quenching of the triplet excimer state by air traces in gaseous argon, *JINST* 3 (2008) P02001. [arXiv:0708.2621](#), [doi:10.1088/1748-0221/3/02/P02001](#).
- [69] D. Y. Akimov, H. Araujo, E. Barnes, V. Belov, A. Bewick, et al., WIMP-nucleon cross-section results from the second science run of ZEPLIN-III, *Phys.Lett. B* 709 (2012) 14–20. [arXiv:1110.4769](#), [doi:10.1016/j.physletb.2012.01.064](#).
- [70] D. Y. Akimov, The ZEPLIN-III dark matter detector, *Nucl.Instrum.Meth. A* 623 (2010) 451–453. [doi:10.1016/j.nima.2010.03.033](#).
- [71] J. Angle, et al., First Results from the XENON10 Dark Matter Experiment at the Gran Sasso National Laboratory, *Phys.Rev.Lett.* 100 (2008) 021303. [arXiv:0706.0039](#), [doi:10.1103/PhysRevLett.100.021303](#).
- [72] E. Aprile, et al., Design and Performance of the XENON10 Dark Matter Experiment, *Astropart.Phys.* 34 (2011) 679–698. [arXiv:1001.2834](#), [doi:10.1016/j.astropartphys.2011.01.006](#).
- [73] E. Aprile, et al., Dark Matter Results from 100 Live Days of XENON100 Data, *Phys.Rev.Lett.* 107 (2011) 131302. [arXiv:1104.2549](#), [doi:10.1103/PhysRevLett.107.131302](#).
- [74] E. Aprile, et al., The XENON100 Dark Matter Experiment, *Astropart.Phys.* 35 (2012) 573–590. [arXiv:1107.2155](#), [doi:10.1016/j.astropartphys.2012.01.003](#).
- [75] E. Aprile, et al., Dark Matter Results from 225 Live Days of XENON100 Data [arXiv:1207.5988](#).
- [76] E. Aprile, et al., Analysis of the XENON100 Dark Matter Search Data, *Astropart.Phys.* 54 (2014) 11–24. [arXiv:1207.3458](#), [doi:10.1016/j.astropartphys.2013.10.002](#).
- [77] E. Aprile, et al., Limits on spin-dependent WIMP-nucleon cross sections from 225 live days of XENON100 data, *Phys.Rev.Lett.* 111 (2) (2013) 021301. [arXiv:1301.6620](#), [doi:10.1103/PhysRevLett.111.021301](#).
- [78] D. Akerib, et al., The Large Underground Xenon (LUX) Experiment, *Nucl.Instrum.Meth. A* 704 (2013) 111–126. [arXiv:1211.3788](#), [doi:10.1016/j.nima.2012.11.135](#).
- [79] S. Moriyama, Status of XMASS experiment, *PoS IDM2010* (2011) 057.
- [80] K. Abe, et al., Light WIMP search in XMASS, *Phys.Lett. B* 719 (2013) 78–82. [arXiv:1211.5404](#), [doi:10.1016/j.physletb.2013.01.001](#).

- [81] H. Uchida, et al., Search for inelastic WIMP nucleus scattering on ^{129}Xe in data from the XMASS-I experiment [arXiv:1401.4737](#).
- [82] X. Cao, X. Chen, Y. Chen, X. Cui, D. Fang, et al., PandaX: A Liquid Xenon Dark Matter Experiment at CJPL [arXiv:1405.2882](#).
- [83] X. Ji, Status of PandaX, Talk at DM 2014, UCLA.
- [84] L. Baudis, A. Behrens, A. Ferella, A. Kish, T. Marrodan Undagoitia, et al., Performance of the Hamamatsu R11410 Photomultiplier Tube in cryogenic Xenon Environments, *JINST* 8 (2013) P04026. [arXiv:1303.0226](#), [doi:10.1088/1748-0221/8/04/P04026](#).
- [85] M. Bossa, DarkSide-50, a background free experiment for dark matter searches, *JINST* 9 (2014) C01034. [doi:10.1088/1748-0221/9/01/C01034](#).
- [86] L. Grandi, DarkSide-50, Talk at DM 2014, UCLA.
- [87] A. Marchionni, et al., ArDM: a ton-scale LAr detector for direct Dark Matter searches, *J.Phys.Conf.Ser.* 308 (2011) 012006. [arXiv:1012.5967](#), [doi:10.1088/1742-6596/308/1/012006](#).
- [88] A. Badertscher, F. Bay, N. Bourgeois, C. Cantini, A. Curioni, et al., ArDM: first results from underground commissioning, *JINST* 8 (2013) C09005. [arXiv:1309.3992](#), [doi:10.1088/1748-0221/8/09/C09005](#).
- [89] K. Rielage, et al., Update on the MiniCLEAN Dark Matter Experiment [arXiv:1403.4842](#).
- [90] M. Boulay, DEAP-3600 Dark Matter Search at SNOLAB, *J.Phys.Conf.Ser.* 375 (2012) 012027. [arXiv:1203.0604](#), [doi:10.1088/1742-6596/375/1/012027](#).
- [91] P. Cushman, C. Galbiati, D. McKinsey, H. Robertson, T. Tait, et al., Snowmass CF1 Summary: WIMP Dark Matter Direct Detection [arXiv:1310.8327](#).
- [92] D. Malling, D. Akerib, H. Araujo, X. Bai, S. Bedikian, et al., After LUX: The LZ Program [arXiv:1110.0103](#).
- [93] L. Baudis, DARWIN: dark matter WIMP search with noble liquids, *J.Phys.Conf.Ser.* 375 (2012) 012028. [arXiv:1201.2402](#), [doi:10.1088/1742-6596/375/1/012028](#).
- [94] R. Agnese, et al., Search for Low-Mass WIMPs with SuperCDMS [arXiv:1402.7137](#).
- [95] H. Kraus, E. Armengaud, C. Augier, M. Bauer, N. Bechtold, et al., EURECA, *PoS IDM2010* (2011) 109.
- [96] T. Alexander, et al., DarkSide search for dark matter, *JINST* 8 (2013) C11021. [doi:10.1088/1748-0221/8/11/C11021](#).
- [97] L. Baudis, DARWIN: dark matter WIMP search with noble liquids, *PoS IDM2010* (2011) 122. [arXiv:1012.4764](#).
- [98] M. Pato, L. Baudis, G. Bertone, R. Ruiz de Austri, L. E. Strigari, et al., Complementarity of Dark Matter Direct Detection Targets, *Phys.Rev. D83* (2011) 083505. [arXiv:1012.3458](#), [doi:10.1103/PhysRevD.83.083505](#).
- [99] J. L. Newstead, T. D. Jacques, L. M. Krauss, J. B. Dent, F. Ferrer, The Scientific Reach of Multi-Ton Scale Dark Matter Direct Detection Experiments, *Phys.Rev. D88* (2013) 076011. [arXiv:1306.3244](#), [doi:10.1103/PhysRevD.88.076011](#).
- [100] L. Baudis, Direct dark matter detection: the next decade, *Phys.Dark Univ.* 1 (2012) 94–108. [arXiv:1211.7222](#), [doi:10.1016/j.dark.2012.10.006](#).